Journal of
Ceramic Science
and Technology

J. Ceram. Sci. Technol. , **08** [3] 365-376 (2017)
DOI: 10.4416/JCST2017-00040
available online at: http://www.ceramic-science.com

Control of Polycondensation Reaction Generated from Different Metakaolins and Alkaline Solutions

A. Gharzouni[1, 2], I. Sobrados[3], E. Joussein[4], S. Baklouti[2], S. Rossignol[*1]

[1]Science des Procédés Céramiques et de Traitements de Surface (SPCTS), Ecole Nationale Supérieure de Céramique Industrielle, 12 rue Atlantis, 87068 Limoges Cedex, France
[2]Laboratoire de Chimie Industrielle, Ecole Nationale d'Ingénieurs de Sfax, Université de Sfax, 3038 Sfax, Tunisia
[3]Instituto de Ciencia de Materiales de Madrid, Consejo Superior de Investigaciones Científicas (CSIC), C/Sor Juana Inés de la Cruz, 3, 28049 Madrid, Spain
[4]Université de Limoges, GRESE EA 4330, 123 avenue Albert Thomas, 87060 Limoges, France
received June 2, 2017; received in revised form August 22, 2017; accepted August 30, 2017

Abstract

The purpose of the present study is to control the polycondensation reaction of various geopolymer samples based on six metakaolins and two potassium alkaline solutions with different reactivities. First, metakaolin characterization revealed three levels of reactivity, which increase essentially with the increase in the degree of purity, amorphous phase and water demand value. The formation of geopolymer samples was then investigated. *In situ* thermal analysis showed that depending on the metakaolin surface reactivity, the availability of dissolved species decreases the energy required for oligomer formation to approximately 1.8 kJ/mol. However, a highly reactive alkaline solution favors the dissolution and decreases this energy to approximately 0.6 kJ/mol, even in the case of low-reactive metakaolins. In addition, *in situ* FTIR spectroscopy revealed that the metakaolin impurities are responsible for the generation of several networks. However, the geopolymer network is favored in the case of a highly reactive alkaline solution. Further, structural information was obtained with *in situ* ^{27}Al NMR. It was proven that the reactivity of metakaolin and, more significantly, the reactivity of alkaline solutions ensure higher conversion rates of $Al^{(VI)}$ and $Al^{(V)}$ species to $Al^{(IV)}$, which may reach 80 %. Better compressive strengths (> 60 MPa) were obtained for high conversion rates.

Keywords: Metakaolin, alkaline solution, kinetics, oligomer formation, ^{27}Al NMR

I. Introduction

With the increasing necessity to develop new construction materials that are environmentally friendly, low-energy-consuming and cost-efficient, geopolymer materials appear as competitive alternative mineral binders. Geopolymers can be defined as three-dimensional amorphous materials derived from the activation of an aluminosilicate source (metakaolin, clays, fly ash, blast furnace slag) by an alkaline solution (silicate solution and alkali hydroxide). Research concerning these materials has been diverse, covering the formation mechanism, working properties and potential applications. Metakaolin was extensively used as an ideal precursor for fundamental studies aiming to explore the kinetics, reaction mechanism and properties of geopolymer materials. In this context, Wang *et al.* [1] summarized the reaction process as first the dissolution of the metakaolin surface layer by NaOH solution and then the polymerization of aluminosilicate species under the effect of monomer, dimer and oligomer species of the silicate solution [2]. Moreover, many authors have tried to explore the geopolymer formation mechanism using different characterization techniques. Furthermore, Provis *et al.* [3] considered that it is difficult to separate each step of the reaction from the other because the steps occur simultaneously and rapidly. Despite this fact, they succeeded in modeling the reaction kinetics using *in situ* energy-dispersive x-ray diffraction. Other authors have used more accurate structural analysis. For instance, Rahier *et al.* [4] studied the reaction kinetics and mechanism using modulated temperature differential scanning calorimetry and dynamic mechanical analysis. They also explored the possibility of ^{27}Al and ^{29}Si NMR to follow the molecular changes during the material synthesis. They found that geopolymers result from complex combined reactions. Indeed, the decrease of OH^- concentration at the beginning of the reaction leads to the formation of an intermediate aluminosilicate species that evolves afterwards to a geopolymer. Recently, Favier *et al.* [5] conducted a heteronuclear liquid NMR study to observe the chemical evolution of the interstitial phase during geopolymerization and correlate it with the evolution of the elastic modulus of the geopolymer paste. A ^{1}H NMR study was also carried out to characterize the geopolymerization

* Corresponding author: sylvie.rossignol@unilim.fr

process of a metakaolin-based geopolymer. The geopolymerization process, in the early stage, was described as a succession of an induction period, an acceleration period, a deceleration period and finally, a stabilization period [6]. Differential thermal analysis (DTA) and thermogravimetric analysis (TGA) during formation have also been useful in determining the geopolymerization rate [7]. The geopolymer samples were maintained at 70 °C for two hours. According to the obtained heat flow curve and associated weight losses, four zones were defined, denoting different reactions: first, the reorganization of species; then, the dissolution of metakaolin, followed by the oligomer formation; and finally, the polycondensation reaction. Despite the existing background models describing the geopolymerization reaction, the mechanism is still the subject of research because it is strongly dependent on the raw materials used. Thus, it is interesting to assess the influence of raw precursor reactivity on the structural evolution of geopolymer materials and their final properties. For this, elucidation of the structural changes as the reaction of geopolymerization proceeds as a function of various metakaolins and alkaline solutions seems to be expedient.

In this paper, the control of the polycondensation reaction will be investigated. The effect of aluminates species from different metakaolins will be studied because they are thermodynamically limiting factors for the polycondensation reaction [8]. The role of silicate species is also important and depends on the alkali cation. Two potassium silicate solutions differing in terms of reactivity were used to exacerbate the effect of alkaline solution reactivity on reaction kinetics. The geopolymer formation was probed by means of differential thermal analysis and thermogravimetric analysis (DTA-TGA), FTIR spectroscopy and ^{27}Al NMR. The mechanical properties of the strengthened materials were then evaluated in compression tests.

II. Experimental

(1) Raw materials and sample preparation

Geopolymer samples were synthesized using six metakaolins (named M1 through M6) (Table 1) and two commercial potassium silicate solutions denoted as S1 and S3 with Si/K molar ratios of 1.75 and 0.65. The total solids ($K_2O + SiO_2$) are equal to 20.7 wt% and 40.6 wt% for S1 and S3 solutions, respectively.

Potassium hydroxide pellets (VWR, 85.2 % pure) were dissolved into the two starting silicate solutions to maintain the Si/K molar ratio at 0.5 during 5 min under magnetic stirring. Then, metakaolins were added. The obtained mixtures were placed in a closed sealable polystyrene mold at room temperature (25 °C). The nomenclature and the composition of the prepared mixtures are reported in Table 2.

Table 1: Chemical and physical properties of raw metakaolins.

Metakaolins	M1	M2	M3	M4	M5	M6
Si/Al	1.17	1.19	1.00	0.98	1.44	1.33
d_{50} (μm)	10	6	8	6	20	26
BET value (m^2/g)	17	22	8	17	18	6
Wettability (μL/g)	760	1250	1010	1186	530	670
Amorphous phase (%)	63	87	98	98	64	59
Heating process	Rotary	Flash	Oven	Flash	Flash	Flash

Table 2: Nomenclature and composition of the studied samples.

Mixtures	Si/Al
S1M1	1.56
S1M2	1.60
S1M3	1.34
S1M4	1.33
S1M5	1.67
S1M6	1.63
S3M1	1.68
S3M2	1.73
S3M3	1.45
S3M4	1.44
S3M5	1.76
S3M6	1.74

(2) Sample characterization

The chemical composition of the raw materials was determined using x-ray fluorescence (ARL 8400, XRF 386 software).

X-ray diffraction patterns were acquired in x-ray diffraction (XRD) experiments on a Bruker-AXS D 5005 powder diffractometer using CuKα radiation ($\lambda K\alpha = 0.154186$ nm). The analytical range is between 5° and 55° (2θ), with a step of 0.04° and an acquisition time of 2 s for raw metakaolin powder. JCPDS (Joint Committee Powder Diffraction Standard) files were used for phase identification. The amorphous phase for each metakaolin was determined with the Rietveld method [9] using Topas software (Brücker). For that, the metakaolins were milled and ground to obtain a particle size smaller than 40 µm. A standard phase (30 % ZnO) was added to the samples.

The particle size distributions of the clays were measured using a laser particle size analyzer (Mastersizer 2000). With this analyzer, powder is suspended by an air current flowing through a glass cell with parallel faces illuminated by a beam of laser light. The measurement is made at a pressure of 3 bars.

Powder BET surface areas were determined by means of N_2 adsorption at -195.85 °C using Micrometrics Tristar II 3020 volumetric adsorption/desorption apparatus. Prior to the measurement, the samples were degassed at 200 °C under vacuum for 4 h.

The water demand value (µL/g) corresponds to the volume of water that can be adsorbed by one gram of powder before saturation. For this, water was added progressively (microliter by microliter) to one gram of metakaolin until saturation, which can be determined when the wetting angle exceeds 90°.

Fourier-transform infrared (FTIR) spectroscopy in ATR mode was used to investigate the structural evolution of the geopolymer mixtures. The FTIR spectra were obtained using a ThermoFisher Scientific Nicolet 380 infrared spectrometer. The IR spectra were acquired over a range of 400 to 4000 cm^{-1} with a resolution of 4 cm^{-1}. The atmospheric CO_2 contribution was removed with a straight line between 2400 and 2280 cm^{-1}. To monitor the geopolymer formation, software was used to acquire a spectrum (64 scans) every 10 min for 13 h. For comparison, the spectra were baseline-corrected and normalized [10].

Differential thermal analysis (DTA) and thermogravimetric analysis (TGA) were performed on SDT Q600 apparatus from TA Instruments in an atmosphere of flowing dry air (100 mL/min) in platinum crucibles. The signals were measured with Pt/Pt-10%Rh thermocouples. Thermal analysis was conducted during the formation of the consolidated materials using the thermal cycle previously established by Autef *et al.* [7]. The fresh reactive mixtures were maintained at 50 °C for two hours.

High-resolution NMR experiments were performed at room temperature on a Bruker AVANCE-400 spectrometer, operating at 104.26 MHz (^{27}Al signal). MAS experiments were carried out for metakaolin powder samples, which were spun at 10 KHz. The number of scans was 400 [9]. For fresh geopolymer reactive mixtures, ^{27}Al NMR in static mode was used. It is well known that ^{27}Al is a quadrupolar nuclei (spin I>1/2). The difficulty of quadrupolar nuclei involves a quick relaxation in the liquid state and a broadening at the first and second order in a solid state, which may limit the quantitative determination of the populations [11, 12]. However, in the liquid state, quadrupolar interaction can be neglected, as previously reported by Favier [13]. The synthesized mixtures were deposited in a zirconia rotor (Ø = 4 mm). A solution of $AlCl_3$ was used as a reference. The ^{27}Al (I = 5/2) NMR spectra were recorded after $\pi/8$ pulse irradiation (1.5 µs) using a 1-MHz filter to improve the signal/noise ratio. In each case, 400 scans were collected. The time between acquisitions was set at 10 s.

The compressive strengths were tested using a LLOYD EZ20 universal testing machine with a crosshead speed of 0.1 mm/min. The compressive strength tests were performed on ten samples for every composition. The samples were cylindrical in shape, with a diameter of 15 mm and a height of approximately 30 mm, and were aged for 7 days in a closed mold at room temperature. Before the tests, the weight and the dimensions of the samples were measured in order to determine the density (ϱ) and therefore the specific compressive strength ($\sigma_\varrho = \sigma/\varrho$).

III. Results and Discussion

(1) Raw metakaolin characterization

To elucidate the main differences between the six metakaolins used, the mineralogical compositions were determined with x-ray diffraction. The resulting XRD patterns are reported in Fig. 1. Whatever the metakaolin, a broad reflection in the $2\theta \approx 20°$ range is observed, characteristic of the typical metakaolin amorphous structure. M1 and M2 show the presence of peaks relative to crystalline phases, such as quartz, residual kaolinite, muscovite and anatase. In the case of M3 and M4, the dome is more pronounced, denoting high structural disorder and a large quantity of amorphous phases. Only traces of quartz were identified in M4. For M5 and M6, the impurity content is higher. Quartz, anatase, calcite and hematite were detected in M5 metakaolin. The presence of hematite was expected from the pinkish color of this metakaolin. M6 is characterized by the presence of mullite in addition to quartz, muscovite, kaolinite and anatase. The presence of mullite can be explained by the over-calcination of particles when these pass near the flame in the case of the flash calcination process as previously detailed by San Nicolas *et al.* [14] and Cyr *et al.* [15]. Thus, the studied metakaolins present different mineralogical phases denoting different purity degrees. Furthermore, the main physical and chemical characteristics of the six metakaolins are reported in Table 1. M1 and M2 have Si/Al molar ratios of approximately 1.17 and 1.19, respectively. M3 and M4 exhibit Si/Al ratios close to 1 (1 and 0.98, respectively), revealing high purity (pure theoretical metakaolin having a Si/Al ratio = 1). However, M5 and M6 have the highest Si/Al ratios (1.44 and 1.33, respectively). This fact is in accordance with the previously discussed mineralogical data. The grain size of each metakaolin was also determined. The d_{50} varies from 6 µm in the case of M4 to 26 µm for M6. The difference in the median diameter from one metakaolin to

another can be explained by the different heating process and pre-treatment [16]. Indeed, all metakaolins were heated at 750 °C but with various processes, as detailed in Table 1. It was demonstrated that the rotary process leads to massive aggregates of particles (the case of M1, for example). However, the flash process produces finer particles with lower agglomeration [17] (the case of M2, for example). The high d_{50} observed in the cases of M5 and M6, despite being heated with the flash process, may be due to the high amounts of accessory minerals, such as quartz. The specific surface area (S_{BET}) is also an important parameter to study because it controls the dissolution rate of metakaolin [18]. Regardless of the metakaolin, the specific surface area values are between 6 and 22 m^2/g, which is in accordance with the literature [19, 20]. M1 and M4 present similar S_{BET} values of approximately 17 m^2/g. M2 and M5 exhibit higher S_{BET} values (22 and 18 m^2/g, respectively), whereas M3 and M6 have lower values (8 and 6 m^2/g, respectively). The differences in the specific surface area between the six studied metakaolins indicate the different structures of the particles [16]. It should also be mentioned that a high specific surface is not always an indicator of high reactivity. Fabri *et al.* [16] mentioned that the dehydroxylation leads to the formation of porous grains. The very small pores can be entered by nitrogen but not by water molecules. Thus, even if the specific surface area is high in this case, the reactive surface is low. That is why the research of another parameter controlling the reactivity is necessary. Recently, Autef *et al.* [9] demonstrated that the water demand value may be a good indicator of reactivity. Thus, it was interesting to compare the water demand values of the studied metakaolins. M1, M6 and M5 show lower water demand values (760, 670 and 530 µL/g, respectively), whereas, M2, M4 and M3 exhibit high water demand values (1250, 1186 and 1091 µL/g, respectively). These differences are linked to different crystallinity of the parent kaolins and various dehydroxylation processes [11]. Finally, the amorphous phase content differs for each metakaolin. As expected, the purest metakaolins (M2, M3 and M4) present the highest amorphous phase content (> 87 %) compared to the others.

For better comprehension of the structural differences between the raw metakaolins, ^{27}Al MAS-NMR experiments were performed. The obtained spectra are presented in Fig. 2.A. All samples exhibit typical ^{27}Al MAS-NMR spectra of metakaolin, showing three main types of components, at approximately 60, 31 and 1 ppm, which are assigned to tetrahedral ($Al^{(IV)}$), pentahedral ($Al^{(V)}$) and octahedral aluminum ($Al^{(VI)}$), respectively [21, 22, 23, 24]. To facilitate the utilization of these data, the obtained spectra were deconvoluted. For example, Fig. 2.B shows three deconvoluted spectra corresponding to M4, M5 and M6. The obtained data concerning the chemical shifts and the percentages of the curve area of the various contributions ($Al^{(IV)}$, $Al^{(V)}$ and $Al^{(VI)}$) relative to the different metakaolins are given in Table 4 A. Broad signals (bands 1, 2, 3 and 4 in Fig. 2.B) with a full-width at half maximum (FWHM) varying between 25 and 40 are associated with metakaolin and reflect the disorder of the structure. However, narrower peaks (band 5, 6, 7 and 8 in Fig. 2.B.b, c) indicate the presence of more crystallized phases. Indeed, a contribution at approximately 2 ppm (FWHM ≈ 10) relative to six coordinated aluminums of muscovite can be detected in all samples (Fig. 2.B.b and c) except M4 (Fig. 2.B.a) and M3 (data not shown). Furthermore, the deconvolution of the M6 spectrum (Fig. 2.B.c) shows the presence of three additional contributions: two peaks at 53.94 and 66.67 ppm (FWHM ≈ 15) that can be assigned to $Al^{(IV)}$ and a peak for $Al^{(VI)}$ at 1.52 ppm (FWHM ≈ 9) revealing the presence of mullite [25] in this metakaolin. This finding is in a good agreement with the XRD data. It also permits a distinction to be made between tetrahedral aluminum coming from impurities (muscovite and mullite) and tetrahedral aluminum relative to metakaolin, which will be the more reactive phase for geopolymerization applications.

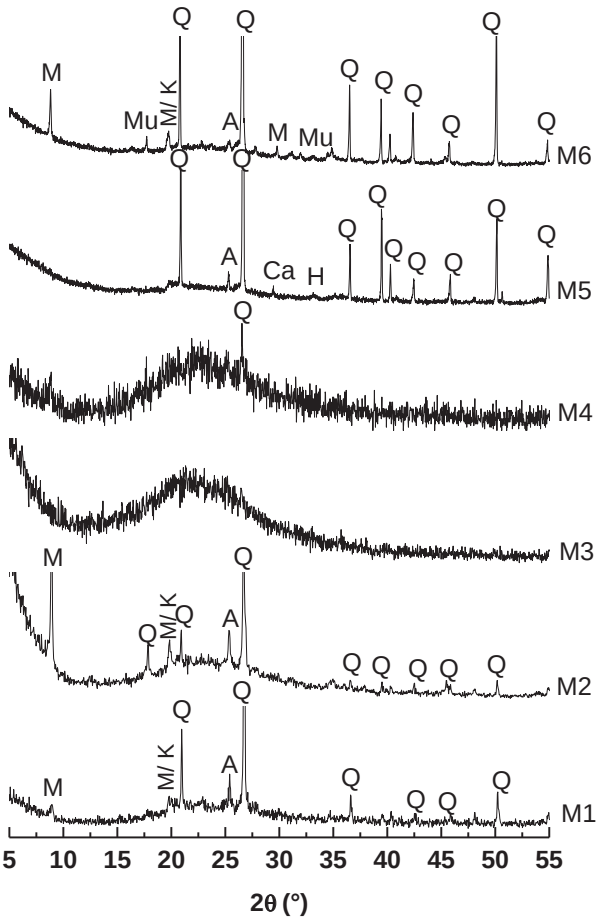

Fig. 1: XRD patterns of the raw metakaolins. The main diffraction peaks are indexed according to the JCPDS files (Q: Quartz (01 – 083 – 2465), K: Kaolinite (00 – 012 – 0447), M: Muscovite (00 – 003 – 0849), A: Anatase (01 – 071 – 1166), H: Hematite (01 – 079 – 1741), Ca: Calcite (00 – 005 – 0586), Mu: Mullite (01 – 089 – 2814)). .

In the light of the metakaolin characterization results, it appears that M2 and M4, followed by M1, have higher water demand values, specific surface areas and reactive tetrahedral aluminum phases, which make them more reactive than the other metakaolins. M3 is very pure and shows interesting properties, but the low specific surface area may likely decrease its reactivity in an alkaline medium. M5 and M6 are the more impure metakaolins and show

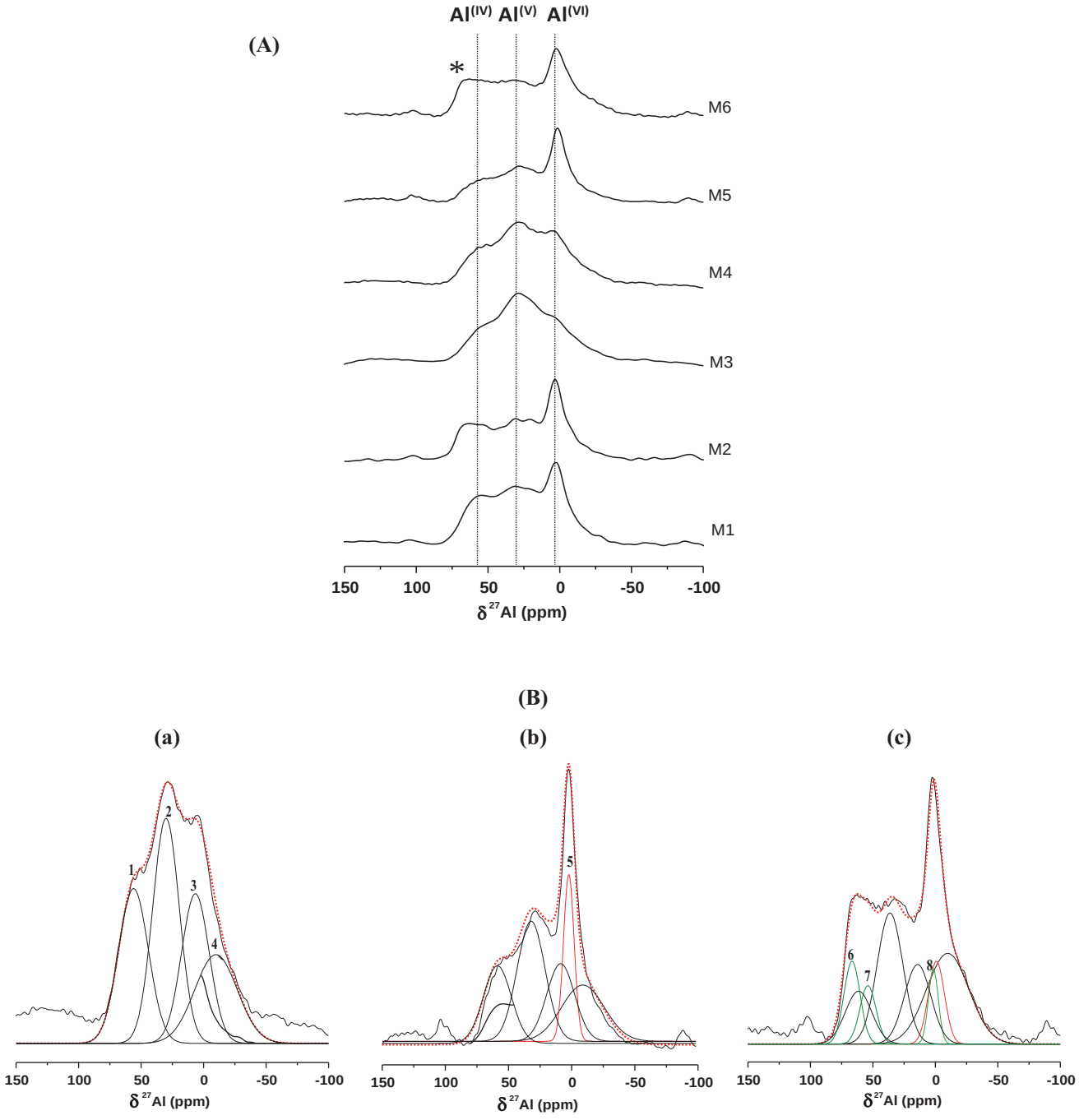

Fig. 2: (A) ^{27}Al NMR spectra of the raw metakaolins (* $Al^{(IV)}$ of mullite) and **(B)** examples of deconvoluted spectra relative to (a) M4, (b) M5 and (c) M6 (Bands 1, 2, 3, 4 are attributed to $Al^{(IV)}$, $Al^{(V)}$, $Al^{(VI)}$ of metakaolin, respectively, band 5 is associated with $Al^{(VI)}$ of muscovite, and bands 6, 7 and 8 correspond to $Al^{(IV)}$ and $Al^{(VI)}$ of mullite).

similar properties. Nevertheless, M5 seems to be more reactive than M6 because it has a higher specific surface area. In summary, the reactivity of metakaolins, which means the ability to release aluminates and silicates species in the alkaline solution, decreases in the order: M2 > M4 > M1 > M3 > M5 > M6.

These hypotheses need to be confirmed in the next sections. Moreover, the effect of the reactivity of metakaolins in the presence of two alkaline solutions, differing in terms of reactivity, on the geopolymer formation and final properties will be exacerbated.

(2) Monitoring geopolymer formation

(a) *In situ thermal analysis*

In the interest of understanding the influence of the reactivity of the starting precursors on the geopolymerization reaction, twelve reactive mixtures, based on the previously characterized metakaolins (from M1 to M6) and two alkaline solutions (S1 and S3), were prepared and studied by means of thermal analysis at 50 °C for two hours. Fig. 3.A presents a typical example of obtained heat flow and weight loss curves for the S1M4 sample

during 120 min of formation. An endothermic peak, associated with a weight loss of 33 %, indicates the occurrence of the different stages of the various reactions. Based on the work of Autef *et al.* [7], four zones can be distinguished according to the inflexion points of the first derivate of the heat flow as schematized in Fig. 3.B. (a, b, c, d for S1M1, S3M1, S1M2 and S3M2, respectively). The first zone corresponds to the reorganization of species to reach speciation equilibrium. The second zone is representative of metakaolin dissolution. Zone 3 is attributed to oligomer formation, and finally, Zone 4 is associated with the polycondensation reaction. In this study, we have focused on the effect of the reactivity of the precursors used on oligomer formation (Zone 3). Extra information can be deduced from thermal analysis curves, such as the time of the beginning of the oligomer formation stage (Fig. 3.B.a) and the energy required for this stage as determined from the heat flow peak area in Zone 3. Examples of the obtained heat flow and first derivate of heat flow profiles during the first 50 min of the reaction are given in Fig. 4 for S1M1, S3M1, S1M2 and S3M2 mixtures. Similar trends are observed, permitting delimitation of the four zones as detailed above. Table 3 summarizes the obtained times and energy values deduced from heat flow curves for each studied sample. Differences are visible depending on the metakaolin and/or the alkaline solution. To compare the different samples, the evolution of the energy as a function of the nAl/t ratio was plotted in Fig. 4, where nAl represents the number of moles of aluminum released from the metakaolin which will be reactive in alkaline media and form oligomers. Regardless of the sample, the energy seems to decrease with a decrease of nAl/t. For S1, a less reactive solution, differences between samples can be considered as a function of the metakaolin used. Indeed, the energy decreases as the nAl/t ratio decreases and as the reactivity of the metakaolin increases. Moreover, the oligomer formation seems to begin earlier (at t ≈ 6.4 min) for less reactive metakaolins (M1, M3, M5 and M6) compared to M2 and M4 (at 7.8 min and 8.6 min for S1M4 and S1M2, respectively). This fact can be explained by the incomplete dissolution of these metakaolins (Zone 2) owing to their lower ability to release aluminates and silicates species and higher stability of impurities, such as mullite, for example, in M6, in an alkaline medium [26]. As a consequence, despite oligomer formation beginning earlier, the lower availability of reactive aluminate and silicate species limits the oligomerization, and more energy is necessary in this stage of formation. However, in the case of more reactive metakaolins, better dissolution is ensured, and the oligomer formation is favored by the high availability and reactivity of the released aluminate and silicate species. This finding is in accordance with the study of Weng *et al.* [18], which highlights the role played by aluminate speciation and $[Al(OH)_4]^-$ ion distribution in promoting geopolymer formation.

Table 3: Beginning time of oligomer formation (t) and energy required for this stage of the reaction (E) determined from heat flow curves of studied samples.

Mixtures	t (min)	E (kJ/Mol)
S1M1	6.4	2.6
S1M2	8.6	1.8
S1M3	6.5	2.5
S1M4	7.8	2.0
S1M5	6.4	3.1
S1M6	6.5	2.5
S3M1	8.3	0.8
S3M2	8.7	0.6
S3M3	8.7	0.8
S3M4	7.9	0.5
S3M5	7.2	0.3
S3M6	8.8	0.8

For S3, a more reactive solution, no significant difference can be detected between the samples. Indeed, the time varies between 7.2 min and 8.8 min, while the energy is between 0.3 kJ/mol and 0.8 kJ/mol. These values are lower than those of the samples based on S1. The role of the high reactivity of the S3 solution is evident. The small depolymerized siliceous species released from this solution are able to enhance oligomer formation and counterbalance the low reactivity of the metakaolins [27].

As a result, it appears that the different stages of the reaction, particularly the oligomer formation, directly depend on the reactivity of the metakaolin as well as the alkaline solution. The surface reactivity of the metakaolin controls the dissolution rate. Thus, the availability of dissolved species influences the kinetics and the energy required for oligomer formation. A highly reactive alkaline solution is able to ensure better dissolution even for low-reactivity metakaolins, which, consequently, favors the oligomer formation. More structural data are required to comprehend the effect of precursors on the reaction rate and the formed networks.

(b) ***In situ FTIR spectroscopy***

To obtain more detailed structural information on the influence of the starting precursors on the reaction rate and the formed networks, ATR-FTIR spectroscopy experiments were performed on the twelve reactive mixtures. This technique has recently shown good potential for monitoring the geopolymer formation at an early age of the reaction [9, 28]. Fig. 5.A gives an example of the FTIR spectral change between t = 0 and t = 400 min for the S3M4 sample. The spectra exhibit two contributions at 3200 and 1640 cm^{-1}, attributed to ν_{OH} and δ_{OH}, respectively. A broad band is also observed in the 1100 – 950 cm^{-1} range and is assigned to the Si-O-M (M = Si, Al) bond. The main change observed over time is the decrease in the intensity of the ν_{OH} and δ_{OH} bands and the shift of the Si-O-M contribution towards lower wavenumbers. This change

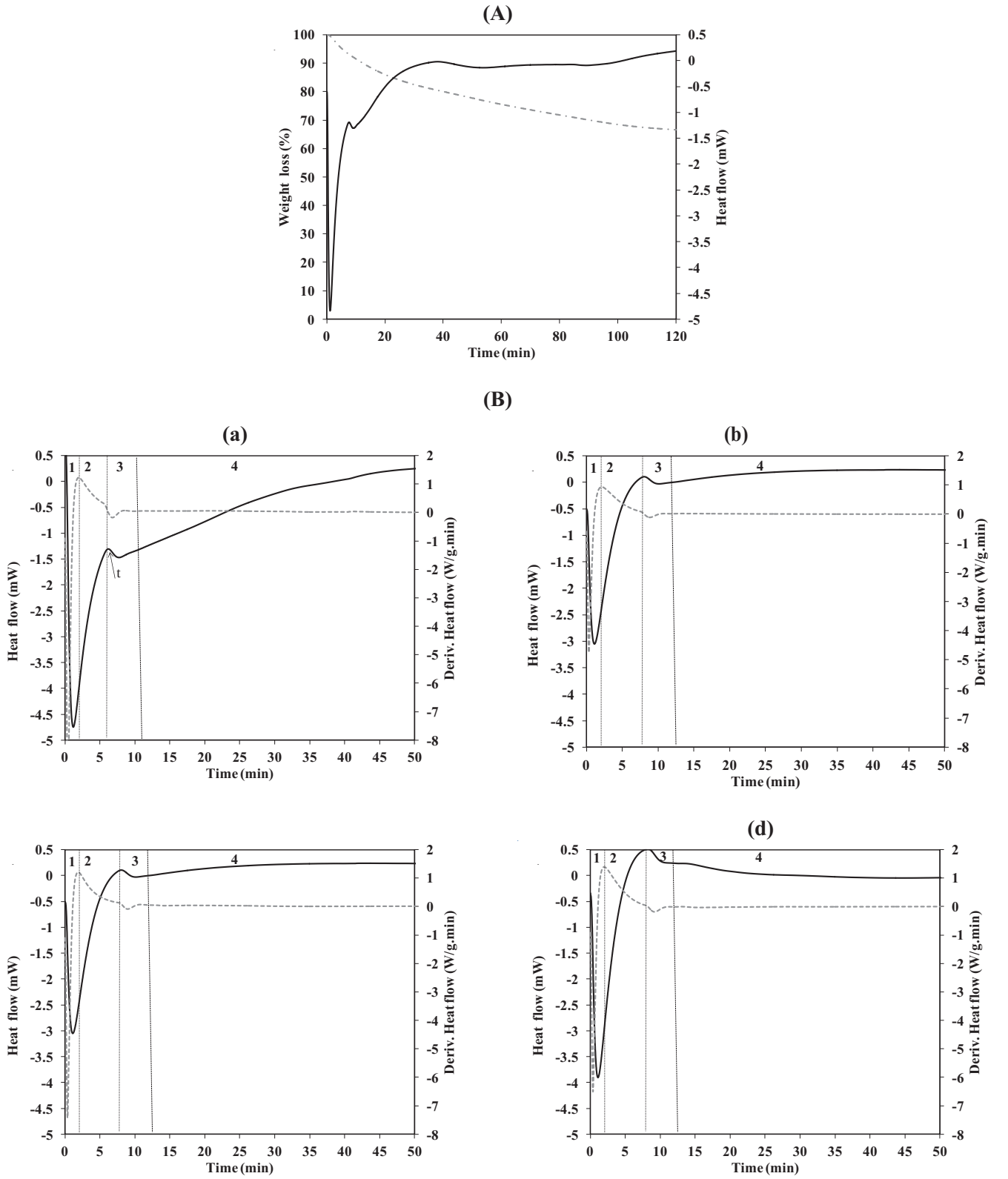

Fig. 3: (A) Typical example of thermal analysis curves and weight loss during 120 min of formation at 50 °C, spectra obtained for S1M4 sample and **(B)** definition of different zones of the reaction for (a) S1M1, (b) S3M1, (c) S1M2 and (d) S3M2 (t = time of beginning of Zone 3).

reveals the occurrence of a polycondensation reaction. The evolution of the Si-O-M band position versus time can be plotted, and the slope at the beginning of the curve can be calculated. The shift value denotes the replacement of Si-O-Si by Si-O-Al bonds during the geopolymerization, and the slope value gives information about the kinetics of the reaction [9, 10].

Fig. 5.B shows the shift values versus (VH_2O_{sol}/VH_2O_{wet}) ·(Δm/(% amorphous·Si/Al)), which represents the ratio of the volume of water supplied by the solution to the volume necessary to wet the metakaolin (calculated according to the water demand values in Table 1) multiplied by (Δm/(% amorphous·Si/Al)), indicating the reactive properties of the metakaolin. It is well known that

the Si/Al molar ratio is a crucial parameter in geopolymerization reaction. In this case, the Si/Al molar ratio was multiplied by the amorphous phase content of metakaolins in order to take into account the structural differences between metakaolins and to consider only the reactive species. Δm is the non-dehydroxylated kaolinite content determined from thermal analysis of the starting metakaolins [9]. Whatever the sample, the shift value increases with $(VH_2O_{sol}/VH_2O_{wet})\cdot(\Delta m/(\%\ amorphous\cdot Si/Al))$. Different behaviors are observed: higher $(VH_2O_{sol}/VH_2O_{wet})\cdot(\Delta m/(\%\ amorphous\cdot Si/Al))$ corresponds to higher shift values in the case of the S1M1 sample. A large shift value (45 cm^{-1}) denotes the formation of different networks, as has been demonstrated in previous work [9, 27]. Indeed, when the M1 metakaolin is activated by S1, a less reactive solution, the volume of water supplied by the solution is much higher than the volume necessary to wet the metakaolin. This fact enables easier species diffusion, as previously demonstrated with thermal analysis during formation, and increases the extent of crosslinking between them. Thus, several networks are formed. The use of S3, a more reactive solution, with the same metakaolin decreases the shift value to 29 cm^{-1} for S3M3. Thus, S3 enhances the formation of a geopolymer phase to the detriment of the other networks [27]. Regardless of the solution used, M2, M3 and M4 exhibit similar shift values varying from 22 to 30 cm^{-1}. These values are characteristic of the formation of a geopolymer phase [9, 29]. These three metakaolins are characterized by a high initial kaolinite amount, then an amorphous phase and water demand values and Si/Al ratios close to 1. Furthermore, the volume of water supplied by the solution seems to be optimal to wet the metakaolin and initiate the reaction. The water volume is important because it controls the driving forces for polymerization [3]. Consequently, the reactivity of the metakaolin and/or alkaline solution favors the formation of a geopolymer network.

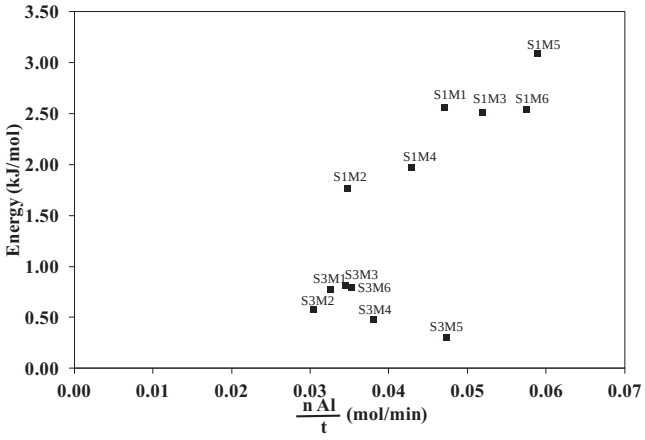

Fig. 4: Evolution of the energy as a function of the nAl/t ratio for each mixture based on various metakaolins and solutions.

In the case of M5 and M6, which are less pure metakaolins, weaker shift values are obtained, especially in presence of S1 (18 cm^{-1} and 15 cm^{-1} for S1M5 and S1M6, respectively). S3 increases these values to 21 cm^{-1} and 22 cm^{-1} for S3M5 and S3M6, respectively. This result is indicative of the formation of a minor geopolymer phase blocked with impurities, such as mullite for M6 and hematite for M5. In fact, these impurities do not participate in the polycondensation reaction and are coated by the alkaline solution [30].

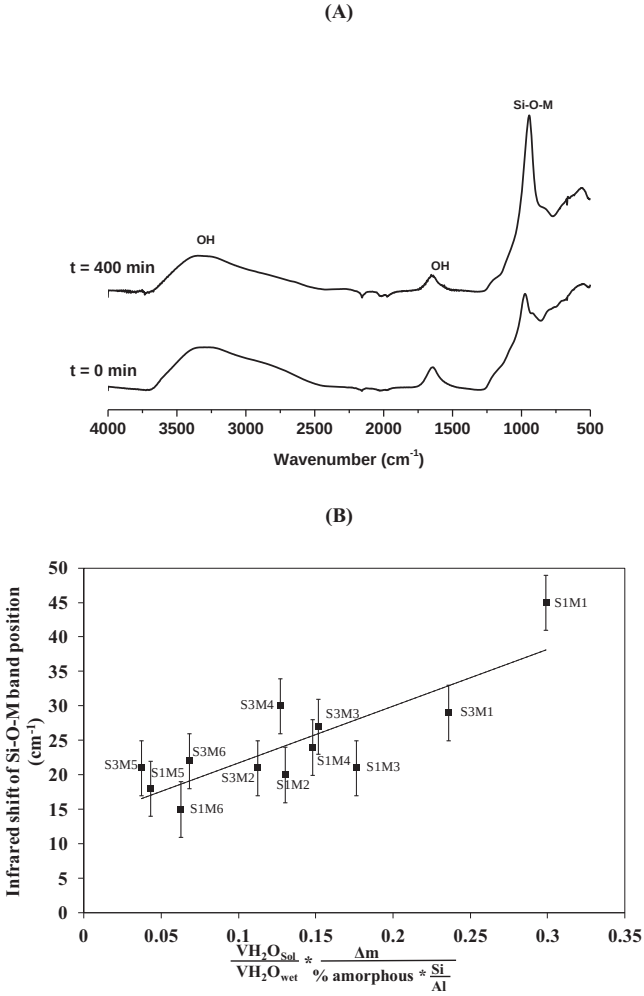

Fig. 5: (A) Example of *in situ* FTIR spectra obtained at t = 0 and t = 400 min for sample S3M4 and **(B)** evolution of the Si-O-M position band shift as a function of $(VH_2O_{sol}/VH_2O_{wet})\cdot(\Delta m/(\%\ amorphous\cdot Si/Al))$.

Thus, regardless of the solution, the metakaolin properties control the nature of the formed networks. The impurity content is also an important factor because of the high resistance of the impurities to alkaline attack. The role of the alkaline solution consists of favoring the geopolymer network as against other possible formed networks. To ensure full comprehension of the reaction rate, NMR analysis is necessary.

(c) *In situ* ^{27}*Al static NMR*

For more detailed structural information about the geopolymer formation depending on the starting precursors' reactivity, the twelve reactive mixtures were studied with ^{27}Al static NMR at different times of the formation (0, 2, 6 and 24 h). Examples of the spectra obtained for the S1M4, S3M4, S1M5 and S3M5 samples are presented in Fig. 6. The obtained data concerning the chemical shifts and the percentages of the curve area of the different contributions are detailed in Table 4B.

Table 4: ^{27}Al NMR data of the various species for **(A)** raw metakaolins obtained with MAS NMR and **(B)** geopolymer reactive mixtures at different times of the reaction obtained with static NMR.

(A)

Metakaolins	Percentage of the area curve of contribution (%)		
	$Al^{(IV)}$ ≈ 60 ppm	$Al^{(V)}$ ≈ 31 ppm	$Al^{(VI)}$ ≈ 1 ppm
M1	18.6	43.4	38.0
M2	21.1	35.7	43.2
M3	24.3	31.3	44.4
M4	24.9	32.3	42.8
M5	18.4	28.6	53.0
M6	24.3	22.8	52.9

(B)

Mixtures	**S1M4**			**S3M4**		
	Percentage of the area curve of contribution (%)					
Time (h)	$Al^{(IV)}$		$Al^{(VI)}$	$Al^{(IV)}$		$Al^{(VI)}$
	≈ 70 ppm	≈ 60 ppm	≈ 10 ppm	≈ 70 ppm	≈ 60 ppm	≈ 10 ppm
0	11.3	24.0	64.7	14.0	19.6	66.5
2	12.2	31.5	56.4	15.1	33.2	51.7
6	2.6	71.9	25.5	2.2	72.8	25.0
24	0.0	81.1	18.9	6.1	83.9	10.0
Mixtures	**S1M5**			**S3M5**		
	Percentage of the area curve of contribution (%)					
Time (h)	$Al^{(IV)}$		$Al^{(VI)}$	$Al^{(IV)}$		$Al^{(VI)}$
	≈ 70 ppm	≈ 60 ppm	≈ 10 ppm	≈ 70 ppm	≈ 60 ppm	≈ 10 ppm
0	17.8	26.8	55.4	6.9	27.0	66.1
2	4.6	43.4	52.0	7.5	48.4	44.1
6	6.0	71.6	22.4	0.0	92.3	7.7
24	8.9	76.3	14.8	0.0	93.2	6.8

Irrespective of the mixture, it was noticed that the spectra are immediately different from those of the starting metakaolins when there is contact with the alkaline solution (from t = 0 h). Indeed, metakaolins show very broad peaks owing to the disorder of the structure. However, for geopolymer reactive mixtures, the peaks become noticeably narrower, indicating a higher degree of structural order [31]. Moreover, the spectra show a dominant phase at approximately 60 ppm, which is characteristic of $Al^{(IV)}$, and a minor broad peak at approximately 17 ppm, corresponding to $Al^{(VI)}$ [32]. In fact, when the metakaolin is mixed with the alkaline solution, an increase of the contribution's area relative to $Al^{(IV)}$ with the disappearance of $Al^{(V)}$ and a remarkable decrease of $Al^{(VI)}$ initially present in the metakaolin are observed. These changes indicate the rapid and strong interaction between the two precursors. As time progresses, the peak relative to $Al^{(IV)}$ broadens, denoting the formation of a geopolymer network, and the intensity of the peak relative to $Al^{(VI)}$ decreases, revealing the dissolution of metakaolin. However, $Al^{(V)}$, which is initially present in the metakaolin, was not observed in any spectra. This fact may be explained by its highly distorted coordination polyhedron or its rapid consumption owing to its high reactivity linked to its strained coordination, as has been previously demonstrated in the literature [22, 33].

The amount of $Al^{(VI)}$ that is still observed in the ^{27}Al spectra of geopolymers even after 24 hours is due to unreacted metakaolin, especially as $Al^{(VI)}$ is more stable and more difficult to dissolve than $Al^{(V)}$ and $Al^{(IV)}$ [31, 22, 34].

Moreover, differences can be distinguished between the percentages of the area curves of the different contributions (Table 4B) as a function of the metakaolins and alkaline solutions used. For example, the use of S3 instead of the S1 solution increases the percentage of $Al^{(IV)}$ species at 24 h from 81.1 to 83.9 % for the M4 metakaolin and from 76.3 to 93.2 % for the M5 metakaolin and at the same time decreases the percentage of $Al^{(VI)}$ species from 18.9 to 10.0 % and from 14.8 to 6.8 % in the case of M4 and M5, respectively. Thus, S3 seems to ensure an easier and more rapid conversion of $Al^{(IV)}$, $Al^{(V)}$ and $Al^{(VI)}$ of metakaolins into $Al^{(IV)}$ in the geopolymer mixture than S1. This fact is more prominent when S3 is combined with a poor-reactivity metakaolin (M5 in this case). These results are in agreement with DTA and FTIR data and confirm that the structural evolution of the geopolymer reactive mixture is strongly dependent on the reactivity of the starting precursors. The role of the aluminosilicate source

is related to the availability of reactive aluminate species (especially $Al^{(IV)}$ and $Al^{(V)}$) initially present in the starting metakaolins, while the influence of the reactivity of the alkaline solution is more important because reactive species released from a highly reactive alkaline solution are more able to attack even poor-reactivity aluminosilicate species to form a geopolymer phase.

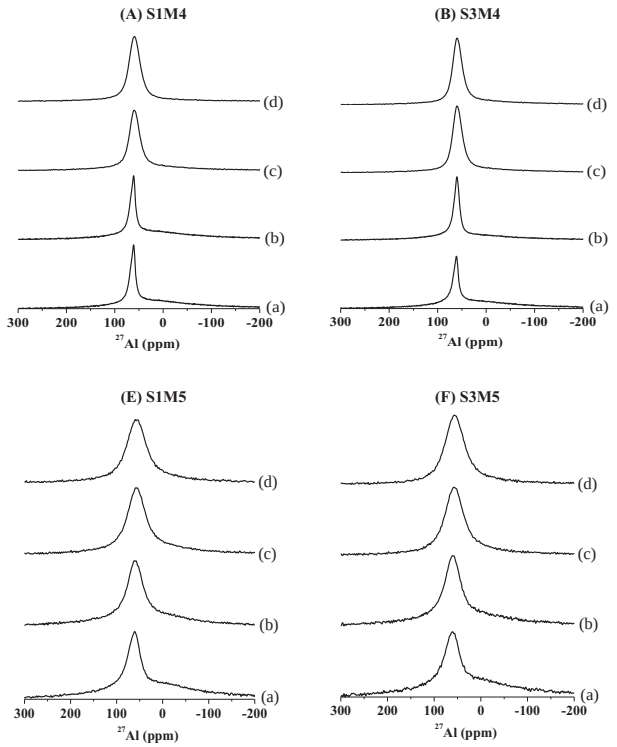

Fig. 6: Recorded ^{27}Al NMR spectra in static mode at (a) 0, (b) 2, (c) 6 and (d) 24 hours of formation for (A) S1M4, (B) S3M4, (C) S1M5 and (C) S3M5 studied samples.

(3) Impact of the metakaolin and alkaline solution on the mechanical properties of the geopolymer

The different behavior of the samples detected by means of thermal analysis, FTIR and NMR experiments during their formation translates into different polycondensation rates depending on the reactivity of the raw materials used and suggest different mechanical properties. To elucidate this effect, the mechanical strengths were evaluated in compression tests. Then, a correlation was established between the $Al^{(IV)}$ formation rate (the difference between the amount of $Al^{(IV)}$ formed after 24 hours in the geopolymer samples and the amount of $Al^{(IV)}$ initially present in the starting metakaolin) and compressive strength data as shown in Fig. 7. Regardless of the sample, it is noted that better compressive strengths correspond to higher $Al^{(IV)}$ formation rates. Moreover, three different behaviors, depending on the reactivity of the used precursors, can be distinguished, as schematized in Fig. 7. For the S1M6 sample, the $Al^{(IV)}$ formation rate did not exceed 62 %, leading to the weakest specific compressive strength value (18 $MPa{\cdot}g^{-1}{\cdot}cm^3$). This fact can be explained by, on one hand, the low surface reactivity of metakaolin. Indeed, M6 has low metakaolin content, reactive $Al^{(IV)}$ and surface area, as detailed previously. On the other hand, the low attack reactivity of the alkaline solution S1 [27] may prevent the formation of $Al^{(IV)}$ species and consequently not allow total alteration of the metakaolin. All of these factors inhibit the formation of a homogeneous geopolymer phase and therefore decrease the mechanical strength.

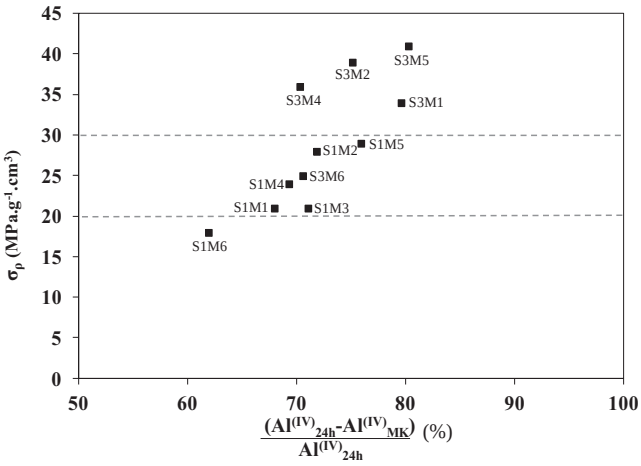

Fig. 7: Evolution of the compressive strength values in function of the $Al^{(IV)}$ formation rate.

The M1, M2, M3, M4 and M5 metakaolins in the presence of the same solution, S1, lead to a higher formation rate of $Al^{(IV)}$, which rises from 67 to 76 %, and increase the specific compressive strength values from 20 to 30 $MPa{\cdot}g^{-1}{\cdot}cm^3$. Thus, the high metakaolin reactivity favors the geopolymer phase and allows the improvement of mechanical strengths. Nevertheless, the S1M5 sample exhibits higher compressive strength despite the low reactivity of the metakaolin. This result can be explained by the high amount of quartz in this metakaolin, which is known to reinforce the geopolymer matrix and increase the strength by providing additional silicon to form Si-O-Si bonds [7, 35].

Finally, for samples using the S3 solution, high formation rates (between 70 and 80 %) were associated with high specific compressive strength values (between 36 and 41 $MPa{\cdot}g^{-1}{\cdot}cm^3$), except for the S3M6 sample (25 $MPa{\cdot}g^{-1}{\cdot}cm^3$). This is due to reactive siliceous species released from the S3 solution being able to ensure a higher metakaolin attack degree induced in this case by the greater formation rate of $Al^{(IV)}$. The contribution of quartz as a reinforcement is evident in the case of S3M5. Nevertheless, the weak compressive strength observed in the case of S3M6 is due to the low reactivity of this metakaolin in addition to the presence of mullite. In contrast to quartz, crystalline phases such as mullite are known to have higher stability in alkaline media, which may hinder the polycondensation reaction, increase the heterogeneity of the sample and consequently decrease the mechanical strength.

IV. Conclusions

The study of the effect of precursors with different reactivity may contribute to better control of the quite complex geopolymerization mechanism. That is why a study was conducted to compare the formation of various samples based on six different metakaolins and two potassium alkaline solutions with different reactivity. First, metakaolin characterization permits the classification of the metakaolins into three groups: most, medium and least reactive depending on the impurity content, amorphous

phase and water demand value. This result was later verified by monitoring the formation of geopolymer samples by means of several techniques. *In situ* thermal analysis reveals that the energy required for oligomer formation in the case of a highly reactive alkaline solution is approximately 0.6 kJ/mol regardless of the metakaolin, while the energy is approximately 1.8 kJ/mol for a highly reactive metakaolin in the presence of a low-reactivity alkaline solution. These results were confirmed by *in situ* FTIR spectroscopy. The metakaolin properties are responsible for the generation of one or several networks. A highly reactive alkaline solution favors the geopolymer network rather than other possible formed networks. *In situ* ^{27}Al NMR measurements supply detailed structural information about the reaction rate of the different mixtures. The role of the aluminosilicate source is related to the availability of $Al^{(IV)}$ and $Al^{(V)}$ in the starting metakaolins, while the role of the reactivity of the alkaline solution is to ensure an easier and more rapid conversion of species, and therefore, the reaction rate can reach 80 %. Finally, a correlation was demonstrated between NMR data during formation and the compressive strength of consolidated materials.

Finally, the obtained results indicated the effect of the reactivity of the precursors on the kinetics and rate of the polycondensation reaction, which is a powerful tool to control the formation and final properties of geopolymers and adapt these to potential applications.

Acknowledgments

The authors gratefully acknowledge Pr. Jesus Sanz for the NMR experiments at the Institute of Materials Science in Madrid.

References

1 Wang, H., Li, H., Yan, F.: Synthesis and mechanical properties of metakaolinite-based geopolymer, *Colloid. Surface*, **268**, 1 – 6, (2005).

2 Granizo, M.L., Varela, M.T.B., Martinez-Ramirez, S.: Alkali activation of Metakaolins: Parameters affecting mechanical, structural and microstructural properties, *Mater. Sci.*, **42**, 2934 – 2943, (2007).

3 Provis, J.L., van Deventer, J.S.J.: Geopolymerisation kinetics. 2. reaction kinetic modelling, *Chem. Eng. Sci.*, **62**, 2309 – 2317, (2007).

4 Rahier, H., Wastiels, J., Biesemans, M., Willlem, R., Van Assche, G., VanMele, B.: Reaction mechanism, kinetics and high temperature transformations of geopolymers, *Mater. Sci.*, **42**, 2982 – 2996, (2007).

5 Favier, A., Habert, G., Roussel, N., d'Espinose de Lacaillerie, J.: A multinuclear static NMR study of geopolymerisation, *Cement Concrete Res.*, **75**, 104 – 109, (2015).

6 Xia, M., Shi, H., Guo, X.: Probing the structural evolution during the geopolymerization process at an early age using proton NMR spin-lattice relaxation, *Mater. Lett.*, **136**, 222 – 224, (2014).

7 Autef, A., Joussein, E., Gasgnier, G., Rossignol, S.: Role of the silica source on the geopolymerization rate: A thermal analysis study, *J. Non-Cryst. Solids*, **366**, 13 – 21, (2013).

8 Provis, J.L., Duxson, P., Lukey, G.C., van Deventer, J.S.J.: Statistical Thermodynamic Model for Si/Al Ordering in Amorphous Aluminosilicates, *Chem. Mater.*, **17**, 2976 – 2986, (2005).

9 Autef, A., Joussein, E., Poulesquen, A., Gasgnier, G., Pronier, S., Sobrados, I. Rossignol, S.: Role of metakaolin dehydroxylation in geopolymer synthesis, *Powder Technol.*, **250**, 33 – 39, (2013).

10 Prud'homme, E., Michaud, P., Joussein, E., Clacens, J.M., Rossignol, S.: Role of alkaline cations and water content on geomaterial foams: Monitoring during formation, *J. Non-Cryst. Solids*, **357**, 1270 – 1278, (2011).

11 Iuga, D., Morai, C., Gan, Z., Neuville, D.R., Cormier, L., Massiot, D.: NMR heteronuclear correlation between quadrupolar nuclei in solids, *J. Am. Chem. Soc.*, **127**, 11540 – 11541, (2005).

12 Man, P.P., Klinowski, J.: Quantitative determination of aluminium in zeolites by solid-state ^{27}AI N.M.R.Spectroscopy, *J. Chem. Soc. Chem. Comm.*, **19**, 1291 – 1294, (1988).

13 Favier, A.: Setting mechanism and rheology of model geopolymer binders, in French, PhD thesis, University of Paris-Est, 2013.

14 San Nicolas, R., Cyr, M., Escadeillas, G.: Characteristics and applications of flash metakaolins, *Appl. Clay Sci.*, **83– 84**, 253 – 262, (2013).

15 Cyr, M., Trinh, M., Husson, B., Casaux-Ginestet, G.: Effect of cement type on metakaolin efficiency, *Cem. Concr. Res.*, **64**, 63 – 72, (2014).

16 Fabbri, B., Gualtieri, S., Leonardi, C.: Modifications induced by the thermal treatment of kaolin and determination of reactivity of metakaolin, *Appl. Clay Sci.*, **73**, 2 – 10, (2013).

17 Medri, V., Fabbri, S., Dedecek, J., Sobalik, Z., Tvaruzkova, Z., Vaccari A.: Role of the morphology and the dehydroxylation of metakaolins on geopolymerization, *Appl. Clay Sci.*, **50**, 538 – 545, (2010).

18 Weng, L., Sagoe-Crentsil, K., Brown, T., Song, S.: Effects of aluminates on the formation of geopolymers, *Mater. Sci. Eng. B.*, **117**, 163 – 168, (2005).

19 Konan, K.L., Soro, J., Andji, J.Y.Y., Oyetola, S., Kra, G.: Comparative study of dehydroxylation/amorphisation in two kaolins with different crystallinity, in french, *J. Soc. Ouest-Afr. Chim.*, **30**, 29 – 39, (2010).

20 Guyot, J.: Measuring the specific surface of clay based on adsorption, in french, *Ann. Argon*, **20**, 33 – 359, (1969).

21 Brown, I.W.M., Mackenzie, K.J.D., Bowden, M.E., Meinhold, R.H.: Outstanding problems in the kaolinite-mullite reaction sequence investigated by ^{29}Si and ^{27}Al Solid-state nuclear magnetic Resonance: 11, high-temperature transformations of metakaolinite, *J. Am. Ceram. Soc.*, **68**, 298 – 301, (1985).

22 Duxson, P., Lukey, G.C., Separovic F., van Deventer, J.S.J.: Effect of alkali cations on aluminum incorporation in geopolymeric gels, *Ind. Eng. Chem. Res.*, **44**, 832 – 839, (2005).

23 Rowles, M.R., Hanna, J.V., Pike, K.J., Smith, M.E., Connor, B.H.O.: ^{29}Si,^{27}Al, ^{1}H and ^{23}Na MAS NMR study of the bonding character in aluminosilicate inorganic polymers, *Appl. Magn. Reson.*, **32**, 663 – 689, (2007).

24 Sanz, J., Madani, J., Serratos, M., Moya, J.S., Aza, S.: Aluminum-27 and Silicon-29 magic- angle spinning nuclear magnetic resonance study of the kaolinite-mullite transformation, *J. Am. Ceram. Soc.*, **71**, 418 – 421, (1988).

25 He, H., Guo, J., Zhu, J., Yuan, P., Hu C.: ^{29}Si and ^{27}Al MAS NMR spectra of mullites from different kaolinites, *Spectrochim. Acta A-M.*, **60**, 1061 – 1064, (2004).

26 Fernandez-Jimenez, A., de la Torre, A.G., Palomo, A., Lopez-Olmo, G., Alonso, M.M., Aranda, M.A.G.: Quantitative determination of phases in the alkaline activation of fly ash. part II: Degree of reaction, *Fuel*, **85**, 1960 – 1969, (2006).

27 Gharzouni, A., Joussein, E., Samet, B., Baklouti, S., Rossignol, S.: Effect of the reactivity of alkaline solution and metakaolin on geopolymer formation, *J. Non-Cryst. Solids.*, **410**, 127 – 134, (2015).

28 Rees, C.A., Provis, J.L., Lukey, G.C., van Deventer, J.S.J.: *In situ* ATR-FTIR study of the early stages of fly ash geopolymer gel formation, *Langmuir*, **17**, 9076 – 9082, (2007).

[29] Gouny, F., Fouchal, F., Maillard, P., Rossignol, S.: Study of the effect of siliceous species in the formation of a geopolymer Binder: Understanding the reaction mechanisms among the binder, wood, and earth brick, *Ind. Eng. Chem. Res.*, **53**, 3559 – 3565, (2014).

[30] Gharzouni, A., Joussein, E., Samet, B., Baklouti, S., Rossignol, S.: Addition of low reactive clay into metakaolin-based geopolymer formulation: Synthesis, existence domains and properties, *Powder Technol.*, **288**, 212 – 220, (2016).

[31] Davidovits, J.: Structural characterization of geopolymeric materials with x-ray diffractometry and MAS-NMR spectrometry. Geopolymer '88 – First European Conference on Soft Mineralurgy, Compeigne, France, Universite de Technologie de Compeigne, 1988.

[32] Fletcher, R.A., MacKenzie, K.J.D., Nicholson, C.L., Shimada, S.: The composition range of aluminosilicate geopolymers, *J. Eur. Ceram. Soc.*, **25**, 1471 – 1477, (2005).

[33] Walther, J.V.: Relation between rates of aluminosilicate mineral dissolution, pH, temperature, and surface charge, *Am. J. Sci.*, **7**, 296 – 693, (1996).

[34] Duxson, P., Provis, J.L., Lukey, G.C., Mallicoat, S.W., Kriven, W.M., van Deventer, J.S.J.: Understanding the relationship between geopolymer composition, microstructure and mechanical properties, *Colloid. Surface A.*, **269**, 47 – 58, (2005).

[35] Atmaja, L., Fansuri, H., Maharani, A.: Crystalline phase reactivity in the synthesis of fly ash-based geopolymer, *Indo. J. Chem.*, **11**, 90 – 95, (2011).